JOTCSA Journal of the Turkish Chemical Society Section: A Chemistry

TURKISH CHEMICAL SOCIETY

Polymeric Nanoparticle Formulation, Characterization and Penetration Study for Topical Delivery of Timolol Maleate

Muhammad Sulaiman[1], Endang Lukitaningsih[2*], Ronny Martien[3], Retno Danarti[4], Yohanes Widodo Wirohadidjojo[4]

[1]Gadjah Mada University, Doctoral Program, Yogyakarta, 55281, Indonesia.
[2]Gadjah Mada University, Department of Pharmaceutical Chemistry, Yogyakarta, 55281, Indonesia.
[3]Gadjah Mada University, Department of Pharmaceutics, Yogyakarta, 55281, Indonesia.
[4]Gadjah Mada University, Department of Dermatology and Venereology, Yogyakarta, 55281, Indonesia.

Abstract: Infantile hemangioma (IH), while usually not life-threatening, often carries the risk of complications and causes anxiety due to changes in appearance. While regarded as an effective therapeutic choice, timolol maleate (TM) is mostly effective for mild and superficial lesions due to its limited absorption. The goal of this study was to examine the potency of natural polymers to be utilized as main ingredients in nanoparticle formulations to be used as a potential alternative for treating IH. The major ingredients chosen for nanoparticle production were chitosan and acacia gum. Different combinations of polymer concentrations were examined to improve the characteristics of an optimal formula. The nanoparticles obtained were assessed in terms of their physical properties, encapsulation efficiency, and skin permeation. The resulting nanoparticles (TMNP) exhibited a spherical morphology, had diameters of 175.417 ± 3.144 nm, a PDI of 0.346 ± 0.031 and ZP of 31.95 ± 1.09 mV. An encapsulation efficiency value of 17.42 ± 0.02% was considerably adequate to promote desirable activity towards IH. The nanoparticle exhibited enhanced penetration of drug compared to the unencapsulated form. This research is hoped to contribute to the expanding application of nanoparticle technology, particularly in the treatment of infantile hemangioma utilizing nanoparticles derived from natural sources.

Keywords: Nanoparticle, Pharmaceutical preparations, Biopolymer, Penetration Study, Infantile hemangioma.

Submitted: November 26, 2024. **Accepted:** April 7, 2025.

Cite this: Sulaiman M, Lukitaningsih E, Martien R, Danarti R, Wirohadidjojo YW. Polymeric Nanoparticle Formulation, Characterization and Penetration Study for Topical Delivery of Timolol Maleate. JOTCSA. 2025;12(2): 117-28.

DOI: https://doi.org/10.18596/jotcsa.1587817

***Corresponding author's E-mail:** lukitaningsih_end@ugm.ac.id

1. INTRODUCTION

Timolol maleate (TM) is a nonspecific beta receptor antagonist that has long been applied to treat cardiovascular diseases (1) and glaucoma (2,3). Recently, TM is also known as one of several potential drugs for the treatment of infantile hemangioma (IH) and has become a subject in many research studies (4). This trend has grown since the incidental finding of oral propranolol activity against IH back in 2008, while it was being used to treat cardiovascular abnormality in infants with IH (5). Regarding the fact that both drugs came from the same family, compared to its predecessor, TM is hypothesized to possess higher potency with lower side effects. Its inhibitory effects are mainly by controlling proliferation via vasoconstriction on hemangioma vascularization controlling angiogenesis (6) and apoptosis induction through beta adrenergic receptor signaling pathways (7) in IH management.

Despite its promising potential, most orally TM is eliminated shortly after being given due to the first pass effect; hence, the poor bioavailability profile (under 50%) (8). On the other hand, a relatively similar activity against IH but with lower side effects is observed in topically applied TM compared to oral propranolol (4) or topical corticosteroids (9). This is due to the fact that topical application can hinder the vast distribution of a drug and avoid many undesired systemic activities. In other research, it was also

proven that concurrent use with oral propranolol can enhance the effects while shortening the duration of medication at the same time (10).

Although timolol's topical dose form is highly effective, it has not been commercially accessible for treating IH. Thus far, numerous investigations and pharmacological trials have exclusively employed ocular drops or simple solutions (11). Moreover, common challenges in conventional topical delivery, such as poor resident time and penetration ability, are also present (12). The outermost layer of the skin, stratum corneum (SC) acts as an obvious obstacle in delivering drug substances, hence limiting the depth of penetration (13). That is why the majority of research regarding topically applied TM only applies to mild superficial and non-complicated conditions of IH. In other research, a topically applied TM still showed mild to medium side effects to the skin condition during treatment. Furthermore, a relatively long term cure is still observed in many cases treated with topical TM (14,15).

Nanotechnology offers a promising way out to solve problems that constantly join topical delivery. Although numerous studies have put forward the use of lipids and surfactants as superior choices due to skin barrier nature (16), natural polymers such as chitosan (CH) offer biocompatibility and penetration enhancing characteristics, which can turn out to be powerful substitutes (17). This research aims to explore the use of entirely natural materials instead of commonly used polyanions like tripolyphosphate (TPP) and poly (lactic-co-glycolic acid) (PLGA) in the production of nanoparticles through ionic gelation. The objective is to improve the effectiveness and safety of topically applied timolol maleate for the treatment of infantile hemangioma. Nanoparticles will be synthesized based on interactions between chitosan (CH) and acacia gum (AG) that occur upon simple stirring. Optimized formula will be obtained using simple lattice design with the help of Design Expert version 11.0 software. Based on the author's current understanding, while numerous studies have examined the application of nanoparticles for drug delivery in IH, this research makes complete use of environmentally friendly and readily obtainable materials and methods, while also employing comprehensive testing protocols as well as competitive results. This raises the possibility that basic nanoparticle technology could be utilized more frequently to improve the prognosis of treatment for infantile hemangiomas.

2. MATERIAL AND METHODS

2.1. Materials

Chitosan medium molecular weight (degree of deacetylation >75%) was purchased from local company CV Bio Chitosan Indonesia (Indonesia), Acacia gum was obtained from Fagron Pharmaceutical (Netherlands), Timolol maleate (99,98% analytical grade) was purchased from Octagon Chemical Limited (China). Acetic acid (99%, analytical grade) and anhydrous sodium acetate from Merck (New Jersey, USA). Ammonium acetate and Acetonitrile were of analytical grade, from Merck (New Jersey, USA) and Smartlab (Indonesia) subsequently.

2.2. Methods

2.2.1. Preliminary study

Each of the nanoparticle constituents was firstly prepared as a stock solution by accurate weighing and solubilizing with appropriate solvents (1% acetic acid for CH, water for AG and TM). Prior to the optimization process, a preliminary trial was conducted without the incorporated drug to find and appropriate working concentration range suitable for the formation of nanoparticles. This was done by creating a matrix table of nanoparticle formation according to the combination of five concentration variations of chitosan (CH) (0,1 - 0,8% w/v) and acacia gum (AG) (0,01- 0,08 % w/v). CH solution was poured into a magnetically stirred glass containing AG solution, both in acetate buffer pH 5 medium, followed by continuous stirring for 10 minutes. The resulting mixture was then observed by visual inspection and continued with size and polydispersity index measurements using particle size analyzer (PSA) Zetasizer Nano (Malvern Instrument, Malvern, UK) to ensure the desired formation of nanoparticles, and the lower and upper limits of working concentrations were determined based on that assessment.

2.2.2. Formula optimization

Optimization process was done by simple lattice mixture experimental method with the help of Design-Expert (Version 11, Stat-Ease Inc., MN, USA) software for further study regarding the effect of each polymer components of the nanoparticle. The two chosen independent variables were the percentage of CH and AG concentrations in the formula. The lower and upper concentrations of CH and AG were obtained from preliminary study results and inserted into the software. The concentration range of both components was then adjusted automatically by the software, as seen in Table I. A total of 11 formulas with five different combinations of CH and AG were acquired and used to synthesize the nanoparticle, this time with the addition of TM as an active component. As for formula F1, F2 and F5 were prepared thrice. A series concentration of AG in buffer pH 5 solution was mixed with drug substance and stirred for 5 minutes to complete the interaction and CH in acetate buffer solution was added subsequently, and the stirring continued for another 10 minutes. The final concentration of TM was fixed to 0,1% for each formula with total polymer of 0,42% (w/v). Desirability value was determined to attain best formula. The resultant formula was thereafter stored at a low temperature of 4º Celsius, while its stability was assessed to verify its suitability for the upcoming test. Assessment was made based on visual inspection (presence of sediment or turbid appearance) followed by size and polydispersity measurement using particle size analyzer instrument Zetasizer Nano (Malvern Instrument, Malvern, UK).

2.2.3. Characterization of optimum formula (TMNP)

Measurements of size and polydispersity index (PDI) can be conducted simultaneously by dynamic light scattering (DLS) method using PSA instrument

Zetasizer nano (Malvern instrument, Malvern, UK). Firstly, samples were prepared by diluting TMNP solution by 1:100 with acetate buffer pH 5. Subsequently, approximately 1 mL sample was put into a glass cuvette and measured at a scattering angle of 90º and a temperature 25º Celsius.

Zeta potential was measured based on the electrophoretic movement of particles upon the presence of electric current using Zetasizer Nano (Malvern instrument, Malvern, UK). Samples were prepared by mixing TMNP solution with acetate buffer at pH 5 in a ratio of 1:100 and placed into a dip cell cuvette for measuring zeta potential. The samples were later measured at a constant temperature of 25º Celsius. Data were collected in triplicate.

The size and morphology of the optimum nanoparticle formation were studied with photography technique using transmission electron microscopy (TEM) instrument (Jeol JEM-1400Flash, USA). This method is using a different technique in determining sizes, so it could also be complementary to size measurement by DLS method. Samples were prepared by a proper dilution of the optimum formula using water. A tiny amount of the sample solution was put on carbon coated copper grid and allowed to evaporate at ambient temperature. Measurement was conducted in vacuum conditions and read at appropriate magnification.

FTIR analysis was conducted to measure and study the possible interaction between components of nanoparticles. This can also be useful to make sure whether the obtained nanoparticles contain each component involved in the formation. For this, a Thermo-Nicolet iS 10 FTIR instrument equipped with a deuterated triglycines sulfate detector was used. A tiny amount of each pure CH, AG and TM powder and freeze-dried TMNP were milled with KBr powder to form a pellets and spectra were recorded between 4000 to 400 cm^{-1}.

Entrapment or encapsulation efficiency (%EE) was determined indirectly, in which the encapsulated drug can be hypothetically determined by measuring the concentration of free drug in the formula. In order to find the concentration of the free drugs, samples were first transferred into a 100 kDa MWCO ultrafiltration tube (Sartorius, Germany). The tube was later centrifuged at 2000 rpm until filtrate was separated and collected to be transferred into a different vial. The filtrate was mixed with mobile phase to reach proper dilution and filtered with 0.45 micron syringe filters and injected into an HPLC instrument with UV detectors. The HPLC system was run on Shimadzu LC-2050C instrument equipped with PDA detectors, using Phenomenex C18 (250 x 4,6 mm; 5 µm) column. A 20 µL diluted sample was injected to HPLC system using acetate buffer pH 3,5/acetonitrile 80:20 as mobile phase, 1 mL/min flow rate, and detection wavelength at 297 nm. All the measurements were done in triplicate and results were expressed in ± standard deviation. The result was marked as free drugs concentration in each formula and % Entrapment efficiency was calculated according to formula:

$$\%\ Entrapment\ Efficiency = \frac{Total\ weight\ of\ drug - Free\ drug}{Total\ weight\ of\ drug}\ x\ 100\ \% \quad (1)$$

2.2.4. Ex-vivo permeation study

To investigate the efficacy of the nano-formulation in facilitating the delivery of timolol maleate across the skin, a permeation study was conducted utilizing the PermeGear ILC07 automated diffusion system instrument (PermeGear, USA). The utilization of rat skin as a membrane barrier involved the collection of samples from euthanized animals, following the clearance of the Ethical Committee of the Faculty of Veterinary Medicine at Gadjah Mada University (EC no 72/EC-FKH/Eks./2023). The obtained skin was stretched onto a surgical tray, and the fat tissue was meticulously separated by the use of a scalpel and surgical blade. Subsequently, the skin was firmly affixed to the membrane bed, featuring a circular diffusion area of 1 cm in diameter. Clamping secured the attachment, orienting the stratum corneum towards the donor compartment. The receptor compartment was filled with a phosphate buffer solution at a constant flow rate, maintaining a pH of 5.5 and temperature at 32 ± 1 ºC. Prior to commencing the test, a 15-minute period was allocated for the purpose of running the instrument, so ensuring the saturation of the skin with a buffer solution. Subsequently, a series of samples (0.5 mL, 200 µg/mL) were subjected to exposure within the donor compartment, initiating the test at a time interval of 6 hours. A volume of 2.4 mL of the sample was collected at regular intervals of 30 minutes. Subsequently, the collected sample was diluted using the mobile phase, followed by filtration using a syringe filter with a pore size of 0.45 microns. Finally, the filtered sample was introduced into the High-Performance Liquid Chromatography (HPLC) system. The HPLC equipment was operated using identical parameters as those employed in the encapsulation efficiency assessment and has been verified to ensure the reliability. The data were subjected to analysis by producing a curve that depicted the accumulation of drugs per unit area as a function of time (18). The values of the steady state or maximum flux (Jss) and the lag time (Tlag) were determined by calculating the slope and x-intercept, respectively, from the linear section of the plot. All study were done in triplicate and data were served as mean ± standard deviation (SD). Statistical significance was determined by two sample T-test with P value < 0.05 was considered statistically significant.

3. RESULTS AND DISCUSSION

3.1. Orientation and Optimization

Timolol maleate nanoparticles (TMNP) were prepared using ionic gelation technique. In this method, nanoparticles are theoretically self-assembled due to ionic interaction between components with opposite charges, which in this case are CH and AG. This

technology has been utilized in the production of polymeric nanoparticles since it is simple and safe for the environment (19). An orientation study was conducted prior to optimization process to simplify the search for optimum concentration range in which nanoparticle was formed. This step was done by mixing CH and AG solutions in several variations of concentration. An acidic aqueous medium was used where the acetyl groups in chitosan's structure and the carboxylate groups of acacia gum are protonated and deprotonated subsequently to make sure the interaction (20). Furthermore, this state was maintained by the use of acetate buffer medium to avoid any pH change. The medium was adjusted to a pH of 5 so that it would be suitable for its intended purpose while avoiding any irritation to the skin's structure.

In the orientation study, nanoparticles were formed in a size of 125.9 to 256.0 nm with PDI between 0.071 and 0.420 (supplementary data). A visually good and desired result of nanoparticle characteristics was seen between the use of CH (0.2-0.4%) and AG (0.02-0.08%). On the contrary, the use of more than 0.4% CH in all ranges of AG resulted in undesirable characteristics such as more turbid solutions with higher size and/or polydispersity index results. It was also worth mentioning that the results became less predictable in that range of concentrations, making it much more difficult to control the outcome of the synthesis. It was concluded that increasing the concentration of CH in a formula produced lower-sized nanoparticles if the concentration of AG was fixed. This result was due to the formation of a more compact and enclosed structure being formed as CH more available. On the other hand, the higher the concentration of AG the bigger the size of the nanoparticle being produced. The reason behind this was because AG as a cross-linker with negative charge tend to be attached in the Np's surface when CH as a counter charge was no more available and apparently this could lead to a bigger size to be formed or trigger aggregation. As an outcome of this preliminary study, a range of 0.1 to 0.4% and 0.02 to 0.06 % for CH and AG subsequently were chosen to be the lower and upper limit working concentration on the next optimization step.

Table 1: Detailed characteristics (Size, polydispersity index (PDI) and zeta potentials (ZP)) of eleven formulas with different combination of chitosan (CH) and acacia gum (AG) in optimization process, n=3.

Formula code	Components (%w/v)			Characteristics		
	CH	AG	TM	Size (nm)	PDI	Zp (mV)
F1	0.4	0.02		172.6 ± 1.131	0.273 ± 0.003	34.1 ± 3.30
F2	0.34	0.08		210.9 ± 1.947	0.137 ± 0.032	39.0 ± 1.27
F3	0.355	0.065		204.3 ± 3.972	0.154 ± 0.004	35.9 ± 2.65
F4	0.4	0.02		175.3 ± 6.647	0.292 ± 0.004	31.0 ± 0.21
F5	0.37	0.05		196.8 ± 1.344	0.188 ± 0.007	40.5 ± 1.41
F6	0.4	0.02	0.1	177.8 ± 0.141	0.252 ± 0.022	34.6 ± 0.98
F7	0.37	0.05		194.1 ± 1.698	0.168 ± 0.004	39.3 ± 1.07
F8	0.385	0.035		189.2 ± 1.935	0.209 ± 0.024	35.5 ± 3.56
F9	0.34	0.08		210.8 ± 2.344	0.124 ± 0.009	40.7 ± 0.65
F10	0.37	0.05		194.3 ± 1.710	0.162 ± 0.018	38.3 ± 0.30
F11	0.34	0.08		211.6 ± 2.192	0.128 ± 0.029	39.7 ± 1.63

In the next step, the obtained lower and upper limits of concentration were used to find the optimum formula and to study the effect of each polymer in the formation of nanoparticles. A total of eleven formulas were determined by the Design-Expert software (Version 11, Stat-Ease Inc., MN, USA) with characteristics after synthesis, as shown in Table 1. A specific criterion was used to determine the most suitable formula: the lowest size and in-range PDI and zeta potential values were expected. Size was considered to be of a higher importance factor since, hypothetically, the lower the size, the better the penetration. Regarding the PDI and zeta potentials, it could be inferred that the optimal formula can be attained when both variables fall within their acceptable range values. The particle size (PS) values were obtained in nanometer range (172.6 ± 1.131 – 211.6 ± 2.192 nm) as seen in Table 1. Adequate precession was 37.96 with adjusted R2 (0.9770) was in reasonable agreement with predicted R2 (0.9684). A linear relationship was built with calculated equation for the PS analysis as seen on equation 1. Positive estimations of X1 (CH) and X2 (AG) suggested a rise in PS when CH and AG concentrations increased. It was also confirmed with the calculated equation that AG possessed much stronger effect on producing bigger size value than CH. The contour plot (Figure 1(a)) demonstrates that the incorporation of different polymer percentages has a direct effect on PS value. Greater CH concentrations yielded lower PS values, whereas higher AG concentrations tended to level up PS values, as determined by preliminary research.

$$PS = 392.38484 .X1 + 982.89766 .X2 \quad (2)$$

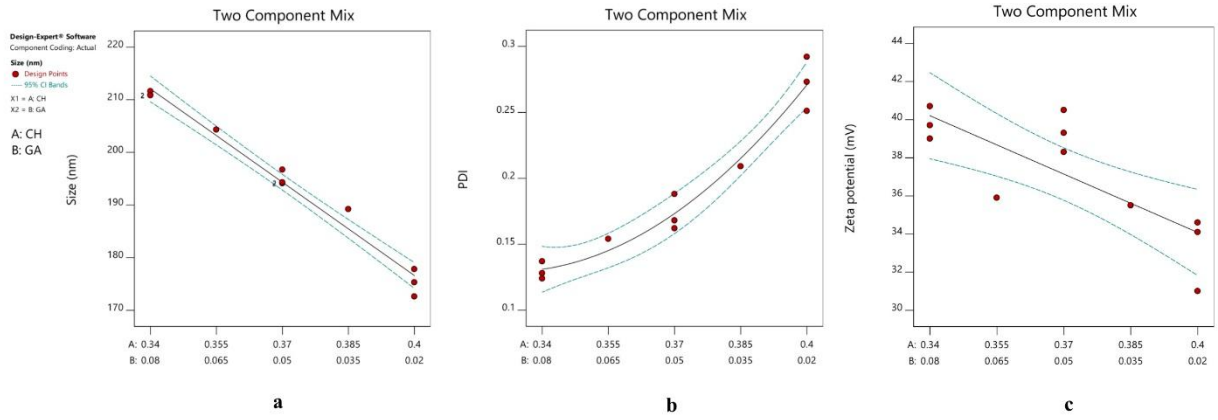

Figure 1: Result on chitosan and acacia gum (CH/AG) mixture at different concentration contour plot graph; Size (a), PDI (b) and Zeta potentials (c).

PDI analysis showed a good polydispersity value (0.124 ± 0.012 – 0.292 ± 0.004) as depicted in Table 1, meaning that the resulting eleven formulas were nearly uniform in size. Adequate precession was 20.05, and adjusted R^2 (0.9490) was in reasonable agreement with predicted R^2 (0.9187). Positive estimates of X_1 and X_2 indicated an increase in PDI as the amounts of CH and AG increased, while the interaction of both components tended to lower the PDI value. This conclusion is true because the interaction of two polymers with different charges tends to produce a more compact and homogenous nanoparticle structure. A quadratic relationship between polymer ratio and PDI was seen in equation 2. From the calculated equation, it can be concluded that AG possessed a stronger effect on producing a higher PDI value than CH and interaction between the two would lower PDI value. The contour plot depicted in Figure 1(b) illustrates the relationship between the inclusion of varying polymer fractions and the resulting impact on the PDI value. Preliminary step findings indicate that an increase in CH concentrations resulted in higher PDI values, while higher AG concentrations were seen to have a tendency to decrease PDI values. The accuracy of this outcome can be attributed to the pivotal role played by AG as the decisive factor in the enhanced production of nanoparticles.

PDI= 0.872862 .X1 + 8.36675 .X2-30.70205 X1.X2 (3)

Zeta potential measurement results can be observed in Table 1 where all the formulas showed varied positive charges (between 30.8 ± 1.00 and 40.7 ± 0.656 mV). These results were reasonable since CH dominates the charge of the formed nanoparticles. Adequate precession was 8.5063, and adjusted R2 (0.5824) was in reasonable agreement with predicted R2 (0.4713). The calculated linear equation was built for the particle size analysis, as seen in equation 3, and it should be highlighted that the interaction of both polymers resulted in a reduction in the positive charge of the nanoparticle core. The results were much more complicated when different combinations of CH and AG were being used, as observed in Figure 1(c). The resultant charge tends to rise and fall depending on the ratio between the two polymers, although all formulas possessed an acceptable range of surface charge.

ZP= 79.29260 .X1-178.34388 .X2 (4)

The results of the optimum formula prediction from the software yield one solution with concentrations of 0.4 and 0.02% (w/v) for CH and AG, respectively, and a desirability value of 0.897. The formula that demonstrates the highest level of efficiency was expected to yield a particle size (PS) value of 176.612 nm, a polydispersity index (PDI) of 0.271, and a zeta potential of 34.084 mV. The model's validity was confirmed through six replicated confirmation attempts of nanoparticle production, resulting in an average size of 175.417 ± 3.144 nm, a PDI of 0.346 ± 0.031, and a ZP of 31.95 ± 1.09 mV.

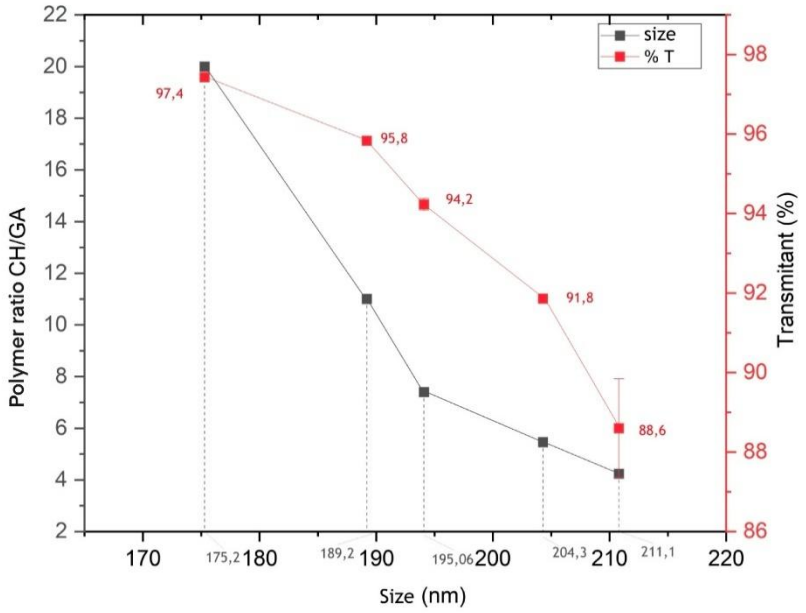

Figure 2: Graph depicting the correlation among polymer ratio, size, and transmittance during the optimization phase.

Visual observation showed a distinct dispersion of nanoparticles without sedimentation (data not shown). This outcome is attributable to the comparatively small amount and size of nanoparticles produced, rendering them invisible to the naked eye. Consequently, alongside ocular observation, transmittance values were obtained utilizing a spectrophotometer within the visible wavelength range of 650 nm. This measurement aims to guarantee the formation of particles in the carrier solution, as a theoretically clear and particle-free solution should yield a transmittance value approaching 100%, allowing nearly all light to pass through the examined solvent layer. The transmittance values measured using a spectrophotometer on nanoparticle samples including various polymer combinations are illustrated in Figure 2. The results indicate that the formation of nanoparticles is characterized by a transmittance value of less than 100%. Moreover, a reduced concentration ratio of CH/GA corresponds to a lower transmittance value. This can possibly be regarded as a consequence of the increased production of nanoparticles. The results indicate that GA is a significant variable in nanoparticle formation, as it serves as a cross-linker that interlinks the CH polymer framework, facilitating the creation of nanoparticles. Furthermore, a negative relationship exists between the size of the produced nanoparticles and the transmittance value; specifically, smaller particle sizes correspond to elevated transmittance values, a phenomenon that can be elucidated by a comparable premise.

Both the material and methods employed in this research offered several advantages. Chitosan and acacia gum in this study are both water-soluble polymers which come from natural sources; hence, they are much more economical and sustainable compared to other materials. Ionic gelation relies only on simple stirring while also avoiding the use of toxic organic solvents, making it known for its ease, cheapness and reproducibility in controlling the desired nanoparticle characteristics. The pH range selected was about 5 because at pH levels below 3.5, the carboxylic groups of GA became protonated, which inhibited the ionic interactions with CH. On the other hand, at pH values above 6.0, close to its pKa, the degree of ionization of Chitosan and its solubility dropped (20). In this study, chitosan and acacia gum were first dissolved in acetate buffer to minimize the pH change during mixing and storing since acidity has a direct effect on the formation of stable chitosan nanoparticles. Moreover, the slightly acidic pH is considered safe and compatible to the natural characteristic of human skin (21).

3.2. Formula Characterization

3.2.1. Size and morphology

In the beginning step of measurements using particle size analyzer, samples were first mixed with their medium (1:100) to reach proper dilution. An acetate buffer with pH 5 was the actual medium of the nanoparticles and has been chosen to dilute the samples; hence, the affecting factors, such as a change in medium viscosity or ionization can be neglected. After the dilution, samples were put in a glass cuvette and measured. The size distribution was obtained and serves as intensity distribution curve, as observed in Figure 3 (a). In addition, the zeta potential graph exhibits a single peak with a narrow band, as seen in Figure 3 (b) which showed ZP value for one of the samples during the optimization process was found to be +34 mV. Adequate stability can be attained, which was supported by the optimal ZP value. This result can later be compared with TEM result. As shown in Figure 4, the morphological properties of the optimized formula were studied using TEM and the photographic view revealed almost spherical particles. The surface of these vesicles looked to be smooth, non-aggregated, and evenly scattered. The

results suggested that such simple synthesis and interaction of two polymers can also creates formation of stable nanoparticles with spherical properties. The TEM micrograph and Zetasizer measurements were in good agreement regarding the mean particle size. As indicated previously, the reported PS was less than 200 nm, which may theoretically achieve good skin penetration and reach the dermis, where IH typically emerges. The dilution step prior to measurement is crucial since DLS method is based on measurement of particles Brownian motion, so it is sensitive to factors affecting the Brownian motion. A very dense particles in its medium can not move freely, thus rated as having a bigger size than the actual size. This can lead to false measurement. This is also applied to aggregated particles. Moreover, as previously explained, the formation of a more numerous and uniform particle population results in a lower PDI value when more AG is present.

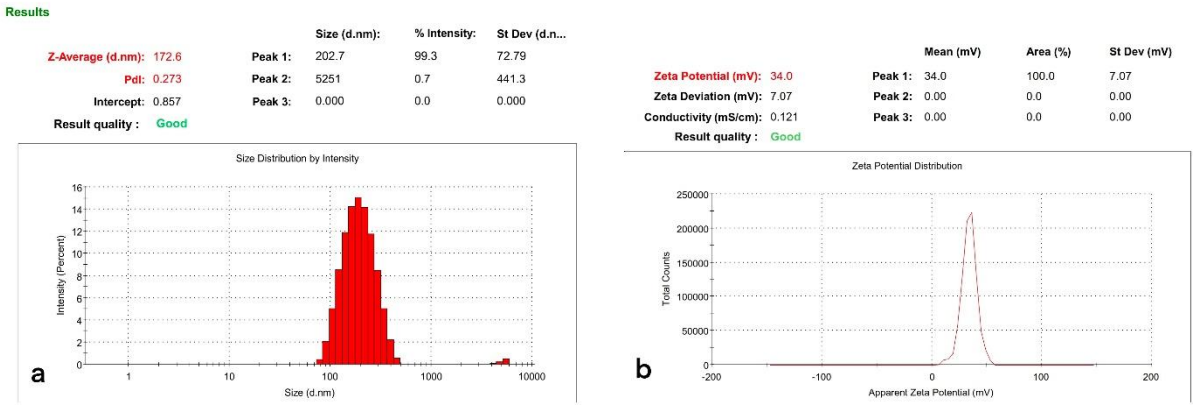

Figure3: Example of Particle size distribution (a) and zeta potential distribution (b) measurement of TMNP formula.

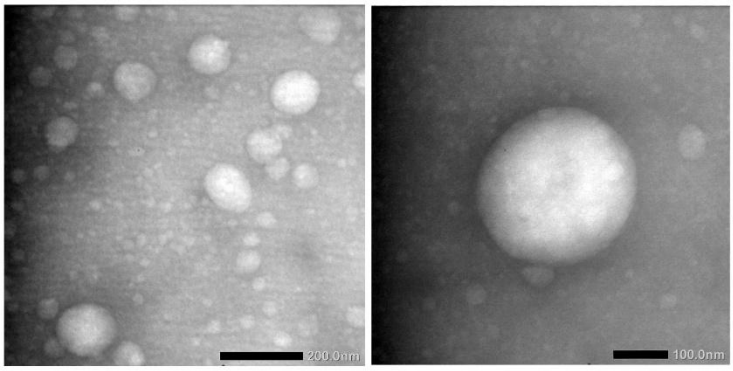

Figure 4: TEM micrograph of optimized formula (TMNP). The morphological properties showed smooth surface and evenly scattered particles with size under 200 nm.

Size is the most unique and important characteristic that defines nanoparticles compared to other delivery systems. Together with its distribution, they both can be determined using dynamic light scattering (DLS) method, which is a principal method employed by particle size analyzer instruments. DLS method collects signals, which are fluctuations of scattering light that happen upon collision between projected light and Brownian moving particles. The signals then transformed mathematically to produce a prediction size of the particle being measured. This definitive size is called hydrodynamic size, which represent hypothetical size of a spherical particle that has the same Brownian motion as the particle being measured (22). That is why results from DLS method are sometimes compared to other methods, such as photography method using Transmission Electron Micrograph (TEM) technique, to ensure the accuracy of the measurement. As for zeta potentials, PSA instrument works based on the measurement of particles' mobility in the event of electric current. In brief, this motion is depicting the surface charge of a nanoparticle and is affected by several factors such as charge of the inner core, ionization of the medium and attached constituent on nanoparticle's surface (23). As a result, zeta potential is a net charge measured as a resultant of those affecting factors. This theory confirms the result in this study where all the zeta potential were in positive value due to CH existence in the core and tend to be lower when more negatively charge AG entangled in the surface of the TMNP. Moreover, the use of acetate buffers as a medium negated the change of TMNP environment that can trigger different particle movements.

3.2.2. FTIR analysis

Each individual component of nanoparticles and TMNP formula itself were analyzed for their structural and possible interactions in nanoparticle formation (Figure 5). Chitosan (CH) powder showed the characteristics of symmetric vibrational bands of -OH and -NH groups at 3376 cm^{-1}. The bands at 2920 cm^{-1} and 2878 cm^{-1} represented C-H stretching vibrations. Since chitosan is not usually fully

deacetylated, there was still a band at 1654 cm^{-1} for the stretching vibrations of C=O (Amide I) followed by the presence of 1598 cm^{-1} band for N-H bending vibration (Amide II). Moreover, stretching vibration of C-O-C in chitosan structure were represented by bands 1077 and 1030 cm^{-1}. This result is in correspondence with another study (24). The acacia gum (AG) spectrum showed a typical band at 3398 cm^{-1} that corresponded to O-H stretching vibration of glycosidic ring, while the band at 2932 cm^{-1} showed the C-H stretching. The C-O stretching vibration of primary alcohol was present at 1070 cm^{-1}. This finding is further corroborated by the outcomes of prior studies conducted by other researchers (25). The CH-AG mixture compounds exhibited a peak at 3419 cm^{-1}, which can be attributed to the stretching vibration of overlapping -NH_2 and -OH groups. Analysis on the CH-AG ionic interaction showed a considerable shift in the carbonyl-amide area due to the interaction of both biopolymers. The N-H bending vibration of -NH_3^+ groups (band at 1598 cm^{-1}) and the asymmetric and symmetric -COO stretching vibrations at 1608 cm^{-1} and 1420 cm^{-1}, respectively, were slightly shifted to 1567 cm^{-1} and 1414 cm^{-1}, suggesting the presence of electrostatic interaction between the amine groups of CH and carboxyl groups of AG. Additionally, the C-N stretching vibration (band at 1154 cm^{-1}) was present but slightly shifted to 1152 cm^{-1}. This finding was also documented in other research publications (26).

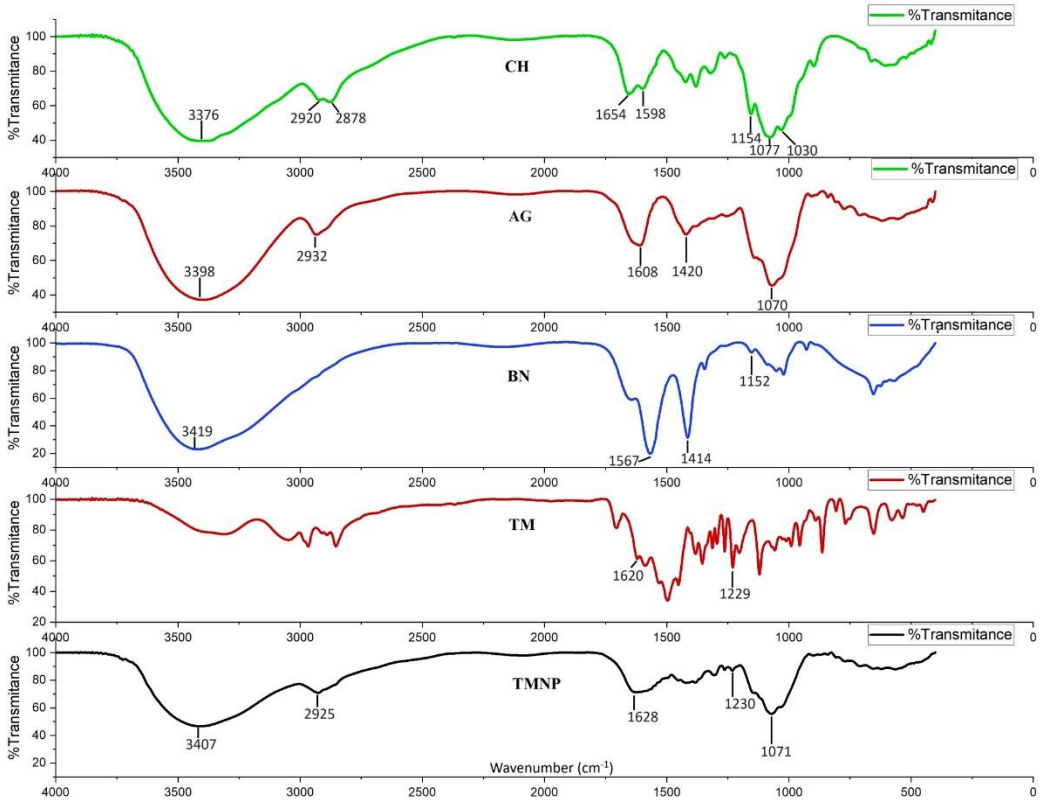

Figure 5: Infra red spectrum analysis of nanoparticles (TMNP) and constituents (CH: chitosan, AG: acacia gum, BN: blank nanoparticle, TM: timolol maleate)

The spectrum of pristine timolol maleate (TM) showed a characteristic broad band of N-H stretching vibration at 3310 cm^{-1} from the secondary amine group. The two weak broad bands at 3046 and 2966 cm^{-1} confirmed the presence of secondary alcohol's O-H stretching. Peaks at 2910 and 2853 cm^{-1} belonged to aliphatic C-H stretching vibration. A strong peak at 1705 cm^{-1} belonged to C=O stretching vibration of the aliphatic carbonyl group of maleic acid. C=N stretching vibration of imine group was observed by the presence of a peak at 1620 cm^{-1}. N-H bending vibration of the secondary amine appeared at 1496 cm^{-1}. A peak appeared at 1229 cm^{-1} belonged to C-N stretching vibration of the secondary amine, while 1202 and 1120 cm^{-1} corresponded to C-O stretching vibration of vinyl ether and secondary alcohol, respectively. Those peaks can also be observed and is comparable to that in several literatures (27). The IR spectra of the TMNP formula, which is a combination of all the analyzed components, exhibits characteristic bands that are also observed in the individual constituent molecules. In summary, the characteristic bands of CH and AG, which indicate the presence of overlapping O-H and N-H stretching vibrations, were observed at 3407 cm^{-1}. Additionally, a band at 2925 cm^{-1}, corresponding to C-H stretching vibrations of polysaccharide components, was observed due to the presence of both polymers. The presence of the C=N stretching vibration of the imine group in the TM structure was confirmed by a shift at 1628 cm^{-1}, compared to the previous value of 1620 cm^{-1}. The C-N stretching vibration of the secondary amine groups was observed at 1230 cm^{-1}, which is a shift from the previous value of from 1229 cm^{-1}. In addition, TMNP exhibited a band at 1071 cm^{-1}, indicating the stretching vibration of the C-O bond in the -OH group of both CH and AG structures.

3.3. Stability on Cold Temperature Storage

Throughout this research, the nanoparticle preparations under investigation were held at low temperatures, and simple stability testing was conducted to establish whether they were appropriate for future study. Table II displays the test results, based solely on two samples. The table shows that the characteristics of the nanoparticles held in the cooler (4 ºC) were similar to those of the freshly synthesized samples even after up to three months of storage (P value > 0.05).

Table 2: Detailed characteristics (size, polydispersity index (PDI) and zeta potentials (ZP)) of samples after 3 month 4 ºC storage.

Samples	Size (nm)		PDI		ZP (mV)	
	Initial	3 months	Initial	3 months	Initial	3 months
TMNP 1	173.7±1.021	174.9±4.743	0.284 ±0.031	0.329±0.064	30.4±1.93	29.9±5.44
TMNP 5	197.4±1.401	199.2±12.89	0.175±0.008	0.220±0.104	40.5±1.41	39.7±1.63

3.4. Entrapment Efficiency

In this study, the determination of %EE was conducted indirectly by measuring free (unentrapped) drug centrifugation technique. The process of isolating unbound drug molecules from nanoparticles is a pivotal stage in the calculation of the percentage encapsulation efficiency. The dialysis method employing a semi-permeable membrane and the centrifugation method utilizing a specific force are the two most commonly employed approaches. The dialysis method is characterized by a significant time requirement, whereas the centrifugation method carries the inherent danger of compromising nanoparticle stability and promoting drug leakage during the procedure. This work used a Vivaspin (Sartorius, Germany) porous tube with a pore size of 100 kDa to facilitate the utilization of low-speed centrifugation and reduce errors. The HPLC method employed in this study has undergone validation and demonstrated its selectivity, accuracy, and precision in quantifying the content of timolol maleate in our nanoparticle samples. Once the free drug has been meticulously extracted from the nanoparticle suspension and appropriately prepared before being introduced into the High-Performance Liquid Chromatography (HPLC) system, the concentration of the free drug may be determined by analyzing the collected samples. The %EE value for the optimal formula was determined to be 17.41 ± 0.015 % based on calculations utilizing the previously stated equation.

3.5. Ex-vivo Penetration Study

In many penetration studies, artificial membranes are frequently employed as substitutes for human skin in penetration tests, mostly driven by ethical considerations. In contrast, several animal models have been proposed as potential substitutes for human skin, encompassing porcine (28), rodent (29), guinea pig, and snake shading skin (30). Nevertheless, these choices present a limitation in relation to the anticipated variation in barrier composition (18). In this study, the ability of polymer nanoparticles to assist timolol maleate penetration was assessed using animal skin (Sprague Dawley rat). The percutaneous penetration profile of timolol maleate in nano-formulation (TMNP) and in solution (TMS) are depicted in Figure 6(a). The figure illustrates that the permeation of TM in nanoparticle group was always greater than that of the naked TM group. It is noteworthy that the disparity in the buildup of permeant became more apparent after a period of 2 hours until the end of the experiment. Moreover, Figure 6(b) clearly illustrates that the nanoparticle group exhibits a higher percentage of drug penetration at the end of experiment. However, the statistical analysis indicated that there were no significant differences between the two groups. This is likely because the test animals were inherently diverse, leading to a wide range of data for each replicate. Nevertheless, this outcome serves as evidence that the benefits of chitosan as a permeation enhancer, particularly in nanoparticle form, significantly contribute to the increased penetration of TM.

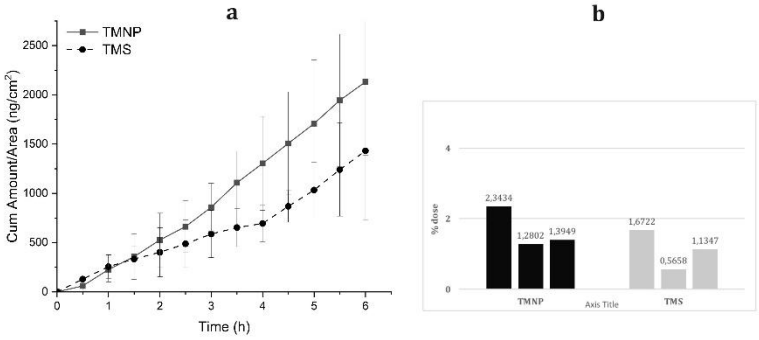

Figure 6: Rat skin penetration profile of timolol maleate nanoparticle (TMNP) and solution (TMS) (a), total penetration served as % dose between TMNP (mean = 1.67 ± 0.58 %) and TMS (mean = 1.12 ± 0.55 &) (b). Data were collected in triplicate and served as mean ± SD.

Timolol maleate, a type of beta blocker, is considered less suited for topical and transdermal application compared to other beta blockers like propranolol and betaxolol (31). A previous experiment has examined the permeation of timolol into human skin using a concentration of 10 mg/mL of timolol maleate. These experiments revealed a minimal penetration rate (1.06 +/- 0.75%) throughout a 4-hour testing period. In addition, the utilization of various permeation enhancers has the potential to significantly increase the absorption of timolol maleate into the epidermis, resulting in a rise from around one percent to multiple times that quantity throughout the 24-hour testing duration (32). In this study, chitosan was utilized as a delivery agent with permeation-enhancing properties. In recent years, significant research has been performed to evaluate the capacity of chitosan and its derivatives to improve permeability. This is accomplished through the use of both bio-adhesion and a transitory rupture of the cellular membrane's tight junctions. Chitosan's cationic nature enables its interaction with the anionic tight junctions of dermal cells, resulting in pore dilatation (33).

Table 3 displays the measured values for flux and lag time of the study. Although the statistical analysis does not show a significant difference between the results of the two samples, it is evident that the average lag time of the TMNP formula is smaller than that of TMS. The steady state flux value exclusively determines the rate at which the drug moves after it has reached a state of saturation in the skin layers, which may not vary significantly once the steady state has been attained. Nevertheless, the lag time value was greater in the TMNP formula, indicating the nanoparticle formula's capacity to enhance penetration. In combination with the shape of the penetration profile curve and the percentage of drug that was transported by the end of the study, it was evident that the nano-formulation improved the delivery of the drug. This study employed rat skin, which offers benefits such as comparable anatomical features to humans and cost-effectiveness and accessibility. Nevertheless, the permeability of mouse skin is comparatively greater than that of human skin so it would be good to conduct further studies using human skin as a comparison (34).

Table 3: Flux (Jss) and lag-time values in timolol maleate penetration study across rat skin in nanoparticle formulation (TMNP) and basic solution (TMS).

Formulation type	Jss ($ng/cm^2.h^{-1}$)	Lag time (h)
TMNP	619.54	0.77
	325.59	0.66
	376.12	0.88
Average	440.41 ± 157.17	0.77 ± 0.11
TMS	620.77	3.66
	166.33	0.68
	295.89	1.28
Average	360.69 ± 234.15	1.87 ± 1.58

4. CONCLUSION

This study demonstrates the successful synthesis of nanoparticles composed of chitosan and acacia gum, utilizing a straightforward technique that eliminates the need for toxic solvents. These nanoparticles were designed to serve as carriers for the drug timolol maleate, specifically for the topical treatment of infantile hemangioma. The effectiveness of this synthesis method was confirmed through various characterization techniques, which collectively provide consistent evidence. This study confirms the feasibility of using a safe biopolymeric incorporation for the treatment of infantile hemangioma, an illness that mostly affects a vulnerable group, mainly infants. Furthermore, the formula exhibits commendable stability for extended periods of storage and possesses an optimal size that facilitates both effective penetration and satisfactory retention inside the skin layer, so ensuring a safer therapeutic approach. The findings of this study provide evidence to endorse the utilization of natural components for enhancing nanotechnology's efficacy in addressing challenges related to medication delivery, particularly in the context of topical treatment for infantile hemangiomas.

5. CONFLICT OF INTEREST

The authors declared no conflict of interest.

6. ACKNOWLEDGMENTS

We expressed our gratitude for the implementation of this research which was carried out through a funding by The Final Project Recognition Grant Gadjah Mada University (Number 5075/UN1.P.II/Dit-Lit/PT.01.01/2023) in 2023.

7. REFERENCES

1. Satterfield KR, Chambers CB. Current treatment and management of infantile hemangiomas. Surv Ophthalmol [Internet]. 2019 Sep 1;64(5):608–18. Available from: <URL>.

2. Cuggino JC, Tártara LI, Gugliotta LM, Palma SD, Alvarez Igarzabal CI. Mucoadhesive and responsive nanogels as carriers for sustainable delivery of timolol for glaucoma therapy. Mater Sci Eng C [Internet]. 2021 Jan 1;118:111383. Available from: <URL>.

3. Negri L, Ferreras A, Iester M. Timolol 0.1% in Glaucomatous Patients: Efficacy, Tolerance, and

Quality of Life. J Ophthalmol [Internet]. 2019 May 2;2019(1):4146124. Available from: <URL>.

4. Wu HW, Wang X, Zhang L, Zheng JW, Liu C, Wang YA. Topical timolol vs. oral propranolol for the treatment of superficial infantile hemangiomas. Front Oncol [Internet]. 2018 Dec 18;8(DEC):605. Available from: <URL>.

5. Tiemann L, Hein S. Infantile hemangioma: A review of current pharmacotherapy treatment and practice pearls. J Pediatr Pharmacol Ther [Internet]. 2020 Sep 1;25(7):586–99. Available from: <URL>.

6. Liviskie CJ, Brennan CC, McPherson CC, Vesoulis ZA. Propranolol for the treatment of lymphatic malformations in a neonate – A case report and review of literature. J Pediatr Pharmacol Ther [Internet]. 2020 Mar 1;25(2):155–62. Available from: <URL>.

7. Macca L, Altavilla D, Di Bartolomeo L, Irrera N, Borgia F, Li Pomi F, et al. Update on treatment of infantile hemangiomas: What's new in the last five years? Front Pharmacol [Internet]. 2022 May 26;13:879602. Available from: <URL>.

8. Morsi NM, Aboelwafa AA, Dawoud MHS. Improved bioavailability of timolol maleate via transdermal transfersomal gel: Statistical optimization, characterization, and pharmacokinetic assessment. J Adv Res [Internet]. 2016 Sep 1;7(5):691–701. Available from: <URL>.

9. Danarti R, Ariwibowo L, Radiono S, Budiyanto A. Topical timolol maleate 0.5% for infantile hemangioma: Its effectiveness compared to ultrapotent topical corticosteroids - A single-center experience of 278 cases. Dermatology [Internet]. 2016 Jan 10;232(5):566–71. Available from: <URL>.

10. Gong H, Xu D peng, Li Y xiao, Cheng C, Li G, Wang XK. Evaluation of the efficacy and safety of propranolol, timolol maleate, and the combination of the two, in the treatment of superficial infantile haemangiomas. Br J Oral Maxillofac Surg [Internet]. 2015 Nov 1;53(9):836–40. Available from: <URL>.

11. Chen ZY, Wang QN, Zhu YH, Zhou LY, Xu T, He ZY, et al. Progress in the treatment of infantile hemangioma. Ann Transl Med [Internet]. 2019 Nov;7(22):692–692. Available from: <URL>.

12. Benson HAE, Grice JE, Mohammed Y, Namjoshi S, Roberts MS. Topical and transdermal drug delivery: From simple potions to smart technologies. Curr Drug Deliv [Internet]. 2019 May 29;16(5):444–60. Available from: <URL>.

13. Ghasemiyeh P, Mohammadi-Samani S. Potential of nanoparticles as permeation enhancers and targeted delivery options for skin: Advantages and disadvantages. Drug Des Devel Ther [Internet]. 2020 Aug 12;Volume 14:3271–89. Available from: <URL>.

14. Püttgen K, Lucky A, Adams D, Pope E, McCuaig C, Powell J, et al. Topical timolol maleate treatment of infantile hemangiomas. Pediatrics [Internet]. 2016 Sep 1;138(3):e20160355. Available from: <URL>.

15. Wu HW, Liu C, Wang X, Zhang L, Yuan W, Zheng JW, et al. Topical application of 0.5% timolol maleate hydrogel for the treatment of superficial infantile hemangioma. Front Oncol [Internet]. 2017 Jun 27;7:137. Available from: <URL>.

16. Zanela da Silva Marques T, Santos-Oliveira R, Betzler de Oliveira de Siqueira L, da Silva Cardoso V, Maria Faria de Freitas Z, Barros RCSA, et al. Development and characterization of a nanoemulsion containing propranolol for topical delivery. Int J Nanomedicine [Internet]. 2018 May 14;13:2827–37. Available from: <URL>.

17. Ma J, Wang Y, Lu R. Mechanism and application of chitosan and its derivatives in promoting permeation in transdermal drug delivery systems: A review. Pharmaceuticals [Internet]. 2022 Apr 10;15(4):459. Available from: <URL>.

18. Neupane R, Boddu SHS, Renukuntla J, Babu RJ, Tiwari AK. Alternatives to biological skin in permeation studies: Current trends and possibilities. Pharmaceutics [Internet]. 2020 Feb 13;12(2):152. Available from: <URL>.

19. Muhtadi WK, Novitasari L, Danarti R, Martien R. Development of polymeric nanoparticle gel prepared with the combination of ionic pre-gelation and polyelectrolyte complexation as a novel drug delivery of timolol maleate. Drug Dev Ind Pharm [Internet]. 2020 Nov 1;46(11):1844–52. Available from: <URL>.

20. Vuillemin ME, Michaux F, Muniglia L, Linder M, Jasniewski J. Gum Arabic and chitosan self-assembly: Thermodynamic and mechanism aspects. Food Hydrocoll [Internet]. 2019 Nov 1;96:463–74. Available from: <URL>.

21. Schafer N, Balwierz R, Biernat P, Ochędzan-Siodłak W, Lipok J. Natural ingredients of transdermal drug delivery systems as permeation enhancers of active substances through the *Stratum Corneum*. Mol Pharm [Internet]. 2023 Jul 3;20(7):3278–97. Available from: <URL>.

22. Modena MM, Rühle B, Burg TP, Wuttke S. Nanoparticle characterization: What to measure? Adv Mater [Internet]. 2019 Aug 30;31(32):1901556. Available from: <URL>.

23. Dukhin AS, Xu R. Zeta-potential measurements. In: Characterization of Nanoparticles [Internet]. Elsevier; 2020. p. 213–24. Available from: <URL>.

24. Akinluwade K, Oyatogun G, Alebiowu G, Adeyemi I, Akinwole I. Synthesis and characterization of polymeric nanoparticles formed from cowry shells and acacia gum extracts. J Adv Biol Biotechnol [Internet]. 2017 Jan 10;14(1):1–8. Available from: <URL>.

25. Ta Q, Ting J, Harwood S, Browning N, Simm A, Ross K, et al. Chitosan nanoparticles for enhancing drugs and cosmetic components penetration through

the skin. Eur J Pharm Sci [Internet]. 2021 May 1;160:105765. Available from: <URL>.

26. de Oliveira JL, Campos EVR, Pereira AES, Nunes LES, da Silva CCL, Pasquoto T, et al. Geraniol encapsulated in chitosan/gum arabic nanoparticles: A promising system for pest management in sustainable agriculture. J Agric Food Chem [Internet]. 2018 May 30;66(21):5325–34. Available from: <URL>.

27. Chavda D, Thakkar V, Soni T, Gandhi T. Formulation and in vitro-in vivo evaluations of timolol maleate viscous eye drops for the treatment of glaucoma. Eur J Biomed Pharm Sci [Internet]. 2016;3(9):573–85. Available from: <URL>.

28. Rahma A, Lane ME, Sinkó B. A comparative study of the in vitro permeation of 2-phenoxyethanol in the skin PAMPA model and mammalian skin. Int J Pharm [Internet]. 2023 Mar 25;635:122692. Available from: <URL>.

29. Todo H. Transdermal permeation of drugs in various animal species. Pharmaceutics [Internet]. 2017 Sep 6;9(3):33. Available from: <URL>.

30. Praça FSG, Medina WSG, Eloy JO, Petrilli R, Campos PM, Ascenso A, et al. Evaluation of critical parameters for in vitro skin permeation and penetration studies using animal skin models. Eur J Pharm Sci [Internet]. 2018 Jan 1;111:121–32. Available from: <URL>.

31. Chantasart D, Hao J, Li SK. Evaluation of skin permeation of β-blockers for topical drug delivery. Pharm Res [Internet]. 2013 Mar 4;30(3):866–77. Available from: <URL>.

32. Soni S, Jain SK, Jain NK. Effect of penetration enhancers on transdermal delivery of timolol maleate. Drug Dev Ind Pharm [Internet]. 1992 Jan 20;18(10):1127–35. Available from: <URL>.

33. Iyer A, Jyothi VGSS, Agrawal A, Khatri DK, Srivastava S, Singh SB, et al. Does skin permeation kinetics influence efficacy of topical dermal drug delivery system? J Adv Pharm Technol Res [Internet]. 2021 Oct 1;12(4):345–55. Available from: <URL>.

34. Supe S, Takudage P. Methods for evaluating penetration of drug into the skin: A review. Ski Res Technol [Internet]. 2021 May 23;27(3):299–308. Available from: <URL>.